Materialia 15 (2021) 100980

Contents lists available at ScienceDirect

Materialia

journal homepage: www.elsevier.com/locate/mtla

Full Length Article

Oxygen vacancies in zirconium oxide as the blue luminescence centres and traps responsible for charge transport: Part II—Films

Damir R. Islamov[a,b,*], Vladimir A. Gritsenko[a,b], Timofey V. Perevalov[a,b], Vladimir Sh. Aliev[a], Vladimir A. Nadolinny[c], Albert Chin[d]

[a] Rzhanov Institute of Semiconductor Physics SB RAS, 13 Lavrentiev Avenue, Novosibirsk 630090, Russian Federation
[b] Novosibirsk State University, 2 Pirogov Street, Novosibirsk 630090, Russian Federation
[c] Nikolaev Institute of Inorganic Chemistry SB RAS, 3 Lavrentiev Avenue, Novosibirsk 630090, Russian Federation
[d] National Chiao Tung University, 1001 University Road, Hsinchu 300, Taiwan

ARTICLE INFO

Keywords:
Zirconium oxide
Defects
Oxygen vacancy
Charge transport
EPR

ABSTRACT

The origin of charge carrier traps in ZrO_2 films was studied using charge transport measurements, EPR spectroscopy and quantum-chemical calculations. After the X-ray irradiation of the ZrO_2 films, the EPR spectra from an interstitial oxygen and a negatively charged oxygen vacancy are observed. The trap thermal and optical activation energies 1.25 eV and 2.5 eV are estimated from the charge transport measurements. Within experiments on the extraction of minority carriers from silicon substrates, it was demonstrated that both electrons and holes can be trapped on oxygen vacancies in ZrO_2. Hence, oxygen vacancies are supposed to operate as traps responsible for the charge transport in ZrO_2 films.

1. Introduction

Crystalline and amorphous films based on zirconium dioxide are of significant interest from a scientific viewpoint, as well as from a practical point of view. The permittivity of different ZrO_2 phases is 15–40. Recently, high-κ dielectric films, like ZrO_2, Al_2O_3, HfO_2, Ta_2O_5, TiO_2 and other ones, were suggested to be used in microelectronic devices as gate dielectrics and active storage layers [1,2]. Also, zirconia is a promising dielectric for the use in the storage capacitor of a Dynamic Random Access Memory cell [3], as well as a storage medium in a terabit scale charge trap flash memory [4,5]. Another ZrO_2-based memory device is a Resistive Random Access Memory (RRAM) cell, which is more attractive that Static and Dynamic Random Access Memories due to its simple structure, low power consumption, high speed operation, and high density integration [6–8]. As far as the charge transport in ZrO_2 is limited by traps, the trap nature in ZrO_2 is the matter of discussion [9,10]. At present, there is a generally accepted hypothesis that oxygen vacancies play a crucial role in the resistive switching, as well as charge localization and transport in ZrO_2, and other high-κ dielectrics. There are a lot of theoretical investigations of oxygen vacancies electronic structure in ZrO_2 [11–16].

The conductivity of dielectrics can be monopolar or bipolar. In the first case either electrons or holes contribute to the charge transport, while, in the second case, both electrons and holes are charge carriers. For example, the conductivity of metal-insulator-semiconductor (MIS) structures with thermal SiO_2 [17] or Al_2O_3 [18] are monopolar (namely, electronic), while HfO_2 [19–21], $Hf_{0.5}Zr_{0.5}O_2$ [22] and TiO_2 [23] are of bipolar conductivity. Non-stoichiometric GeO_x films exhibit the bipolar conductivity, whereas stoichiometric GeO_2 films, after a post deposition annealing, are of monopolar electronic conductivity [24]. Thus, the contribution of electrons and holes to the charge transport in ZrO_2 and the transport mechanism are subjects to be studied.

This paper addresses the origin of the traps responsible for the charge transport and their correlation with paramagnetic centres in ZrO_2.

2. Experimental methods

2.1. Preparation of samples

The electron paramagnetic resonance (EPR) spectra were recorded for 50 nm thick ZrO_2 films on the silicon substrate Si (100). The samples were prepared by the ion beam sputtering deposition on a high-resistance silicon substrate with the resistance of 5000 Ω·cm, as described in Ref. [25]. The substrate at room temperature was placed near the metal zirconium target. High-purity oxygen was delivered to the substrate area, while the target was bombarded by Ar+ ions. The substrate heating, due to the interaction with hot carriers from the target, did not exceed 70 °C. For the purity of the experiments on the high tempera-

* Corresponding author at: Rzhanov Institute of Semiconductor Physics SB RAS, 13 Lavrentiev Avenue, Novosibirsk 630090, Russian Federation.
E-mail address: damir@isp.nsc.ru (D.R. Islamov).

https://doi.org/10.1016/j.mtla.2020.100980
Received 22 September 2020; Accepted 4 December 2020
Available online 11 December 2020

ture annealing effect, a silicon plate with deposited films was divided into two fragments. One of them was X-ray irradiated and the resulting paramagnetic states were studied. The second fragments of the plates were pre-annealed at 1100 °C, and then the samples were studied by EPR before and after X-ray irradiation. To increase the oxygen vacancies concentration and remove interstitial oxygen, part of the samples were annealed at a high temperature (1100 °C) for two hours in the nitrogen atmosphere. The post-deposition annealing was performed in a quartz reactor. The heating and cooling phases were slow. The samples were taken out from the reactor after cooling to room temperature. A possible formation of SiO_2 interfacial layer at the Si/ZrO_2 interface might be confirmed by observing the E' centre in SiO_2, because we cannot separate its signal from the quartz holders one. To create charged paramagnetic oxygen vacancies, the initial samples and those annealed at a high temperature were X-ray irradiated on a general purpose diffractometer (DRON) with a copper anticathode at room temperature for two hours. The structural properties of the as-deposited ZrO_2 dielectric were examined by a grazing incidence X-ray diffraction diffractogram (GI-XRD), and the structural analysis showed that the resulting ZrO_2 films were amorphous. The structural analysis was not carried out for the annealed films, but one can assume that, after the high-temperature treatment, recrystallization occurred in the monoclinic phase [16] or in a mixture of different phases, including tetragonal or even cubic, due to the large surface area to the bulk ratio for thin films [26].

The transport measurements were performed for test MIS structures $Ni/ZrO_2/Si$ on silicon substrates. The 20-nm thick zirconia films were deposited on n-(100) 4.5 Ω·cm and p-type Si (111) 10 Ω·cm wafers by physical vapour deposition (PVD). A pure ZrO_2 target was bombarded by an electron beam in a high vacuum chamber, and ZrO_2 was deposited on the wafer. No post-deposition annealing was applied to prevent the SiO_2 sub-layer forming. The structural analysis showed that the resulting ZrO_2 films were amorphous. All samples for transport measurements were equipped with round 50-nm-thick Ni gates with the radius of 70 μm.

2.2. EPR measurements

The EPR spectra were recorded in the X-band frequency range of the modified Varian E-109 spectrometer at room temperature. To improve the signal-to-noise ratio in the EPR spectra, the number of spectral scans was varied from 300 to 1000. A quartz holder was used for the reference E' centre.

2.3. Transport measurements

The DC current–voltage ($J - V$) curves were measured using a Hewlett Packard 4155B Semiconductor parameter analyser at temperatures 25–175 °C.

The carriers charge sign in semiconductors can be found by measuring the Hall effect and thermoelectric power. These methods are not applicable to dielectrics due to the very low mobile charge carriers density. The carriers charge sign in dielectrics can be found from experiments on the injection of minority carriers from n- and p-type silicon in MIS structures [27,28] or on separating the electrons and holes of the total current in an MOSFET [20,29]. The non-equilibrium minority holes might be injected into dielectrics from the n-Si substrate under illumination, as well as non-equilibrium minority electrons might be injected into dielectrics from the p-Si substrate under illumination [19,23,24]. In the present work, the minority carriers are extracted from n- and p-Si in the equilibrium states at different temperatures.

In this case, according to the mass action law, electron and hole densities (n_s and p_s, respectively) in the thermodynamic equilibrium state of a semiconductor are related as

$$n_s p_s = n_i^2, \tag{1}$$

where n_i is the intrinsic carrier density. Assuming that the major carrier density (electron) is constant within the experimental temperature range, and

$$n_i \sim T^{3/2} \exp\left(-\frac{E_g}{2kT}\right), \tag{2}$$

where T is temperature, E_g is the bandgap in the semiconductor substrate and k is the Boltzmann constant, one can conclude that the minority carriers current has exponentially increases with the growing temperature:

$$J_h^* \sim p_s \sim T^{\alpha} \exp\left(-\frac{\epsilon}{kT}\right), \tag{3}$$

where J_h^* is the current of holes as minority carriers, α is a constant and ϵ is an activation energy that take into account the temperature dependencies of charge-carrier densities, probability of injection on the semiconductor-dielectric and dielectric-metal interfaces, and other factors that contribute to the current of minority carriers.

It should be noted that Eqs. (1) and (2) are applicable for semiconductors, and we use them in (3) just to evaluate the charge current through a dielectric layer qualitatively. Thus, if the current of the MIS structure with the n-Si substrate in depletion mode demonstrates its exponential dependence on temperature, then the dielectric layer exhibits the hole conductivity.

Similar considerations can be made for an MIS structure with a p-Si substrate. In this case, if the current of electrons as minority carriers exponentially depends on temperature, the dielectric layer exhibits the electron conductivity.

In dielectrics with monopolar conductivity, the transport is described by Shockley–Read–Hall equations:

$$\frac{\partial n}{\partial t} = +\frac{1}{q}\nabla \cdot \vec{J}_f - \sigma v n\left(N - n_t\right) + n_t P_{ion}, \tag{4}$$

$$\frac{\partial n_t}{\partial t} = +\frac{1}{q}\nabla \cdot \vec{J}_t + \sigma v n\left(N - n_t\right) - n_t P_{ion}, \tag{5}$$

where n is the density of 'free' electrons in the conduction band, t is time, q is elementary charge (absolute value), $\vec{J}_f$ is the current of 'free' electrons, σ is the trap capture cross-section, v is the electron drift velocity, N is the bulk trap density, P_{ion} is the trap ionization rate, n_t is the density of trapped electrons, $\vec{J}_t$ is the current of trapped electrons without ionization into a conduction band. The total current is $\vec{J} = \vec{J}_f + \vec{J}_t$. In case of a large number of traps in dielectrics, the current of free electrons is negligible due to low n values [30]. In the one-dimensional static case with the uniform distribution on charge traps ($a = N^{-1/3}$), the Eqs. (4) and (5) give the final current–voltage characteristics:

$$J = qan_t\left(1 - \frac{n_t}{N}\right)\left(P_{tun}^{\leftarrow} - P_{tun}^{\rightarrow}\right) - qa^2\frac{P_{tun}^{\leftarrow} + P_{tun}^{\rightarrow}}{2}\frac{\partial nt}{\partial x}, \tag{6}$$

where a is the mean distance between neighbour traps, $P_{tun}^{\rightarrow}$ and $P_{tun}^{\leftarrow}$ are rates of charge carriers hopping between traps without ionization into conduction (valence) band along and against the electric field, x is the coordinate. The first term in Eq. (6) is the drift current, the second one is the diffusion current. In the stationary case, the current values can be calculated as described in Ref. [31]:

$$J_{stat} = qN\frac{a}{4}\left[P_{tun}^{\leftarrow} - P_{tun}^{\rightarrow}\right]\left[1 + \tan^{-2}\gamma(\Omega)\right], \tag{7}$$

where

$$\Omega = 2\frac{a}{d}\frac{P_{tun}^{\rightarrow} + P_{tun}^{\leftarrow}}{P_{tun}^{\rightarrow} - P_{tun}^{\leftarrow}}$$

is the dimensionless number that characterizes the trapped charge spatial distribution in the stationary state, d is the dielectric layer thickness, $\gamma(\chi)$ is the implicit function which satisfies the following equation:

$$\gamma\tan(\gamma) = \chi^{-1}.$$

Recently, it has been demonstrated that the Phonon-Assisted Tunnelling of Electrons (and holes) between Neighbour Traps (PATENT) model [32] adequately describes the current in high-κ dielectrics

[21,22,33]. According to this model, the rate of the tunnel junction between neighbouring traps is the following:

$$P_{\text{tun}} = \int_{\varepsilon>0} \frac{\hbar\varepsilon}{m^* a^2 kTQ_0} \exp\left(-\frac{(Q-Q_0)^2-(Q-qFa/Q_0)^2}{2kT} - \frac{4}{3}\frac{\sqrt{2m^*}\left(\varepsilon^{3/2}-(\varepsilon-qFa)^{3/2}\right)}{qF\hbar}\right)dQ,$$
$$-\varepsilon = -Q_0(Q-Q_0) - W_{\text{opt}},$$
$$Q_0 = \sqrt{2(W_{\text{opt}}-W_{\text{t}})}, \quad (8)$$

where $\hbar$ is the Planck constant, m^* is the electron effective mass, Q is the configuration coordinate of a 'trapped-electron-with-phonons' system. Here '$-\varepsilon$' represents the energy (below conduction band bottom E_c) of a trapped electron interacted with phonons, and Q_0 is the configuration coordinate characterizing the electron-phonon interaction.

In case of low electric fields $eFa \ll W_t$, Eq. (8) can be simplified to

$$P_{\text{tun}} = \nu \exp\left(-\frac{W_{\text{opt}}-W_{\text{t}}}{2kT}\right) \times \exp\left(-\frac{2a\sqrt{2m^*W_{\text{t}}}}{\hbar}\right)\sinh\left(\frac{qFa}{2kT}\right). \quad (9)$$

Here, the pre-exponential factor ν is the attempt-to-escape frequency:

$$\nu = \frac{2\sqrt{\pi}\hbar W_{\text{t}}}{m^* a^2 Q_0\sqrt{kT}}. \quad (10)$$

The first exponent represents the thermal ionization with the activation energy of $(W_{\text{opt}}-W_{\text{t}})/2$, the next exponent is the tunnelling factor and the last term indicates the activation energy decreasing due to the external electric field. Using Eqs. (6) and (9) one can extract the largest distance between neighbouring traps from the slope of experimentally measured currents in the $\log(J)$-vs-F plate.

The analysis shows that, in moderate and strong electric fields ($qFa \geqslant \frac{1}{4}W_t$), Eq. (9) gives a significant deviation, and Eq. (8) should be used.

In case of bipolar conductivity, Eqs. (4) and (5) should be extended with a system of the same equations for holes. The electron–hole recombination should be taken into account as well.

2.4. Ab-initio *simulations*

The ZrO_2 electronic structure was investigated within the density functional theory with the BPE0 exchange-correlation functional. The plane-wave cutoff energy was taken equal to 70 Ry, and the potentials of nuclei and core electrons were described by optimized norm-conserving Vanderbilt pseudopotentials [34,35]. The oxygen vacancies were simulated by removing an oxygen atom from the 96-atom supercell of monoclinic (m-) ZrO_2, respectively. The simulations were carried out using the Quantum ESPRESSO code [36].

The thermal W_t and optical W_{opt} trap electron ionization energies of oxygen vacancy V^q with charge q ($q = -2, -1, 0, 1$) are estimated as follows:

$$W_{\text{t}}(V^q) = \left(E_{\text{p}}^{-1} + E_{\text{d}}^{q+1}\right) - \left(E_{\text{p}}^{0} + E_{\text{d}}^{q}\right), \quad (11)$$

$$W_{\text{opt}}(V^q) = W_{\text{t}}(V^q) + \left(E_{\text{d}(q)}^{q+1} - E_{\text{d}(q+1)}^{q+1}\right). \quad (12)$$

Here E_{p}^{q} and E_{d}^{q} are the total energies of the perfect and defect supercell with the total charge q in the optimized geometry, respectively; $E_{\text{d}(q)}^{q+1}$ is the energy of the supercell with charge $(q+1)$ calculated in the geometry corresponding to charge state q. W_t corresponds to a transition to the ground (relaxed) state, W_{opt} corresponds to a vertical transition from the occupied defect ground state to the excited (non-relaxed) empty state.

Table 1
The calculated W_t and W_{opt} (in eV) values for oxygen vacancies in five charge states in m-ZrO_2 with the schemes of the corresponding excitation.

	Coord.	V_O^{+1}	V_O^{0}	V_O^{-1}	V_O^{-2}
		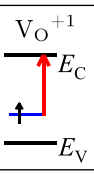	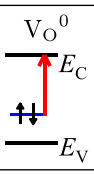	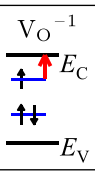	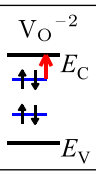
W_t/W_{opt}	3-c	1.7/2.5	1.4/2.0	0.2/0.3	0.6/0.6
	4-c	2.0/3.0	2.0/2.5	0.7/1.0	0.3/0.3

3. Results

3.1. *Defect nature identification:* ab initio *simulations*

The thermal trap energy values W_t, calculated by Eq. (11), can be interpreted as an energy gain when the electron is localized on the defect. Positive W_t values indicate that the charge carriers localization on 3- and 4-coordinated V_O is energetically favourable (Table 1). The charge density distribution and W_t values indicate that V_O in m-ZrO_2 can act as an electron and hole trap and, thus, be involved in the charge transport. However, the asymmetry of Kohn–Shem level positions and spatial charge distributions show that the holes exhibit the localization in the V_O stronger than electrons. This conclusion can be generalized for amorphous and polycrystalline ZrO_2, since the electron properties of solids are determined by a short-range order [37,38]. This is consistent with the fact that the V_O is the key defect responsible for the high-κ dielectric conductivity.

The calculated W_t values in Table 1 can be compared with the experimental ones that were obtained from charge transport studies: 1.15 eV [39] 1.25 eV (will be discussed below), and also with the thermal trap energy values 1.2 eV and 1.33 eV obtained in the TSL experiment. The calculated W_t values for V_O^0 and V_O^{-1} are in a reasonable agreement with the experiments considering the features of the calculation method. The error value in this kind of calculations is greater than that for the Kohn–Shem level positions due to the background charge compensation affects on the supercell total energy values. The calculated W_{opt} values are also affected by the simplicity of the excited state calculation model and, as a result, the expected equality $W_{\text{opt}} = 2W_t$, that takes place for SiO_2 [40], Al_2O_3 [18], HfO_2 [21,33], $Hf_{0.5}Zr_{0.5}O_2$ [22] and other dielectrics, is not satisfied.

3.2. *Defect nature identification: EPR methods*

The EPR study was carried out for ZrO_2 films before and after X-ray irradiation. The first sample with the initial ZrO_2 film on a silicon substrate exhibits no paramagnetic centres. The X-ray irradiation of the sample gives rise of two features in the EPR spectrum, as shown in Fig. 1.

To determine the g-factors for the observed centres, the E' centre in quartz with $g = 2.0005$ was used as a reference. The simulations of the paramagnetic centres induced by X-ray irradiation show (Fig. 1) that they can be described by the spin-Hamiltonian $\hat{H} = \beta\hat{g}\hat{H}\hat{S}$, where $S = 1/2$, the main values of the g-factor for the first centre are $g_{\parallel} = 2.0378$, $g_{\perp} = 2.004$, and for the second one are $g_{\parallel} = 1.958$, $g_{\perp} = 1.964$. Similar EPR spectra with the identical g-factors were observed in ZrO_2 bulk and film structures and correspond to the manifestation of interstitial O_2 centres, and negatively charged oxygen vacancies [41–43]. It should be noted, that the first centre with $g_{\parallel} = 2.0378$, $g_{\perp} = 2.004$ can be a surface-adsorbed superoxide ion O_2 [42,43].

Taking the ZrO_2 density of 6 g/cm^3, the sample volume of 2.5×10^{-5} cm^3, molar mass of ZrO_2 123 g/mol, the EPR method sensitivity of 10^{10} at the line width 6 G, one can find the charged oxygen vacancy density in about 1 ppm.

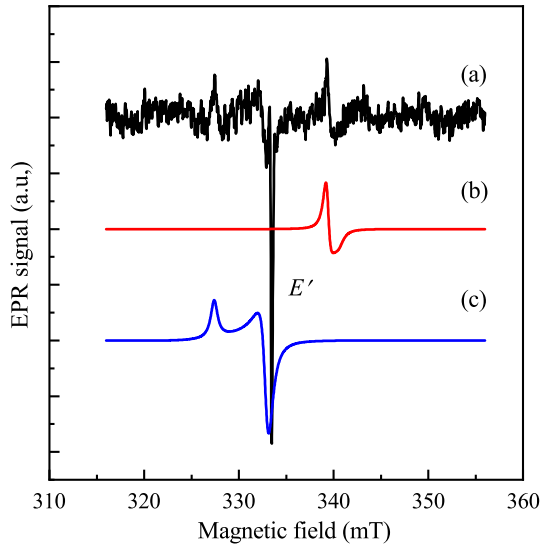

Fig. 1. The EPR spectra of the ZrO_2 film after X-ray irradiation. (a) The experimental spectrum. (b) Simulations of a negatively charged oxygen vacancy with $g_{\parallel} = 1.958$, $g_{\perp} = 1.964$. (c) Simulations of an interstitial O_2 with $g_{\parallel} = 2.0378$, $g_{\perp} = 2.004$). The *E'* centre in quartz is taken as a reference for the *g*-factor with $g = 2.0005$.

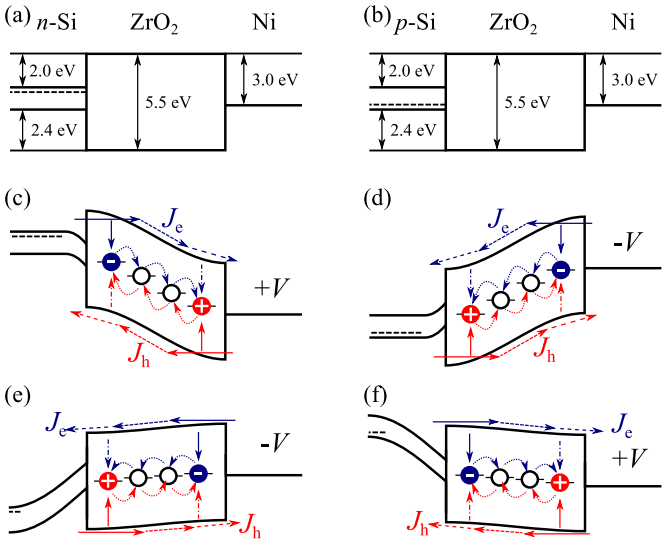

Fig. 2. Energy band diagrams of the $Ni/ZrO_2/Si$ structures: (a) the $Ni/ZrO_2/n$-Si structure in the flat band mode; (b) the $Ni/ZrO_2/p$-Si structure; (c) The energy band diagram of the $Ni/ZrO_2/n$-Si structure in the accumulation mode ($V > 0$); (d) the $Ni/ZrO_2/p$-Si structure in the accumulation mode ($V < 0$); (e) the $Ni/ZrO_2/n$-Si structure in the depletion mode ($V < 0$); (f) the $Ni/ZrO_2/p$-Si structure in the depletion mode ($V > 0$). Here J_e and J_h are the flows of the electrons and holes, respectively, injected into ZrO_2; J_e^* and J_h^* are the flows of the minority carriers (electrons and holes, respectively) injected from Si into ZrO_2.

After the high-temperature annealing at 1100 °C of the second ZrO_2 sample, the EPR spectra exhibit no features in the signal. X-ray exposure of annealed ZrO_2 fragment on a silicon substrate does not lead to the appearance of EPR spectra.

To summarize, the X-ray irradiation of ZrO_2 films on a silicon substrate transforms interstitial oxygen atoms and oxygen vacancies into a paramagnetic centre.

3.3. Charge transport and trap parameters in ZrO_2

3.3.1. Injection of minority carriers

In this section we report on the charge carrier sign determination in ZrO_2-based MIS structures using experiments on the minority carriers injection from *n*-Si and *p*-Si substrates.

In Fig. 2(a) and (b) is the energy band diagrams in the flat band mode of the $Ni/ZrO_2/n$-Si and $Ni/ZrO_2/p$-Si structures, respectively, based on the photoemission data and photoconductivity measurements [44]. The energy barrier for electrons on the Si/ZrO_2 interface is 2.0 eV, and the barrier for holes is 2.4 eV. The energy barrier for electrons on the Ni/ZrO_2 interface is 3.0 eV [45].

A set of experimental $J - V$ characteristics of $Ni/ZrO_2/n$-Si structures measured at different temperatures T is shown in Fig. 3(a). The positive voltage ($V > 0$) corresponds to the positive bias on the Ni contact. In this case, the most part of the applied voltage falls on ZrO_2, the leakage current through ZrO_2 grows with an increase of the electric field (applied voltage) and temperature in the accumulation mode (Fig. 2(c)). The analysis of this regime will be discussed in the next section. In the depletion mode, i.e. when a negative potential is applied to the metal contact, the current is increased exponentially at low voltages. The current saturation appears at a sufficiently large voltage $V \lesssim -2$ V, and the saturation current level increases with the growing temperature. These phenomena indicate that, in the depletion mode, the minority carriers are injected from Si into ZrO_2. The minority carriers are holes in case of the *n*-Si substrate.

On the other hand, the temperature growth might lead to an increasing of the electron injection from the metal contact to ZrO_2 within Schottky [46] or other mechanisms (J_e in Fig. 2(e)). However, the current saturation indicated that it is the minority carriers in the silicon substrate the charge transport through ZrO_2 is limited by.

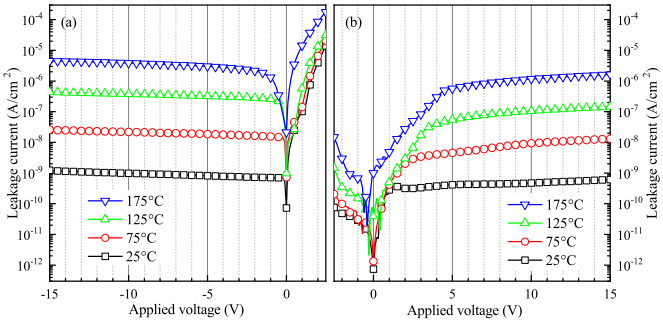

Fig. 3. Experimental current–voltage characteristics of $Ni/ZrO_2/Si$ structures at different temperatures in the depletion mode. (a) The $Ni/ZrO_2/n$-Si structure, (b) the $Ni/ZrO_2/p$-Si structure.

The experimental $J - V$ characteristics for $Ni/ZrO_2/p$-Si MIS structures are shown in Fig. 3(b). In the accumulation mode ($V < 0$), the current grows exponentially with the increasing voltage. In the depletion mode, at a low voltage, the current grows exponentially with the increasing voltage. At $V \gtrsim +3$ V, the electron system falls into the inversion mode, the current saturation appears, and the saturation level increases with the growing temperature. The similar arguments, as shown by Eqs. (1)–(3), are suggestive of the minority-carrier (electrons in this case) current in the depletion mode exponentially depends on temperature. This phenomenon indicates the electron injection from the silicon substrate into ZrO_2 (J_e^* in Fig. 2(f)). However, it should be noted that the same phenomenon might take place in the case of hole thermal injection from the Ni contact (J_h in Fig. 2(g)).

In the conclusion of this section, the charge transport in ZrO_2 is bipolar. Both electrons and holes contribute to the charge current in this material. The obtained results are consistent with *ab initio* simulations, namely, with the fact that the oxygen vacancy in ZrO_2 is a trap for both electrons and holes, as well as with the experiments on the non-

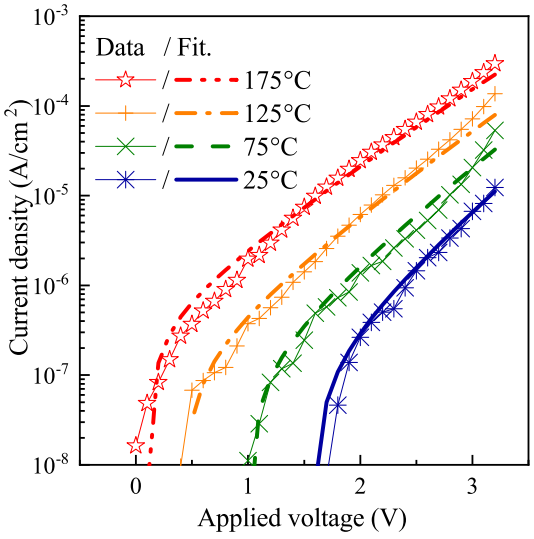

Fig. 4. Experimental (characters) and calculated, in terms of the PATENT model (lines), current–voltage characteristics of Ni/ZrO_2/*n*-Si structures at different temperatures.

equilibrium minority carriers injection under illumination from silicon substrates to perfect single-crystal ZrO_2 films [47].

3.3.2. Charge transport mechanisms

The current–voltage characteristics of the Ni/ZrO_2/*n*-Si structure, measured at different temperatures T, are shown in Fig. 4 in the semi-log plate by characters. The current depends on the applied voltage and temperature exponentially, as expected according to Eqs. (6) and (9). The best congruence of the calculated $J - V - T$ curves with the experimental data is achieved with the following PATENT model parameter values: $W_t = 1.25$ eV, $W_{opt} = 2.5$ eV, $N = 2.1 \times 10^{19}$ cm^{-3} and $m^* = 0.2m_0$, where m_0 is the free electron mass. In case of the uniform trap distribution, the obtained trap density corresponds to the mean distance between traps $a = 3.62$ nm, which is small enough to dominate the tunnelling between traps over the trap ionization into the conduction band.

It should be noted that the experimental data on charge transport can be described in terms of Frenkel model [48] qualitatively. However, the quantitative agreement of experimental data with simulations can be achieved only in case of non-physical parameter values [33].

4. Discussion

The charge transport in ZrO_2 is described by the phonon assisted tunnelling between traps, as well as in HfO_2 and $Hf_{0.5}Zr_{0.5}O_2$ [22,33,49]. The thermal trap energy in ZrO_2, HfO_2 and $Hf_{0.5}Zr_{0.5}O_2$ is equal to 1.25 eV, and it is equal to the half of the Stokes blue luminescence shift in both ZrO_2 and HfO_2 [16,25]. Hence, one can conclude that the oxygen vacancy is the defect responsible for the charge transport in ZrO_2, HfO_2 and $Hf_{0.5}Zr_{0.5}O_2$. The presence of oxygen vacancies in ZrO_2 films is demonstrated by EPR spectroscopy.

The configuration diagram of trap ionization on a negative charged oxygen vacancy is shown in Fig. 5. The lower term corresponds to the initial state of the phonon-coupled trap with an electron before the tunnelling act. The upper term represents the final state of electron-free trap after the tunnelling to the neighbouring trap. The direct (optical) transition energy is 2.5 eV, while the minimal excitation (thermal transition) energy is 1.25 eV. It is interesting to note, that the thermal trap energy of 1.25 eV is equal to a half of the Stokes shift in blue photoluminescence of ZrO_2 crystals and films.

Despite the fact that the charge transport in ZrO_2 is bipolar, the monopolar model describes the experimental data with a good quantitative agreement. This can be explained by the fact that one type of charge carriers has the major contribution to the current, while the contribution of another carrier type is negligible due to the larger barriers at the semiconductor-insulator and metal-insulator interfaces, as shown in Fig. 2(a) and (b), and their injection into the dielectric layer is suppressed. Another possible reason is caused by the differences in the electronic structure of the defects for localized electrons and holes.

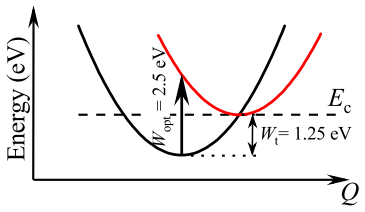

Fig. 5. Configuration coordination energy diagram of trap ionization on a negative charged oxygen vacancy in ZrO_2. The lower black term refers to the filled ground state, and the upper red term does to the empty excited state.

On the other hand, the transport in ZrO_2 is bipolar indeed, but the electron and hole traps must have the same parameters (W_t, W_{opt}, m^*). In this case, the transport might be described in terms of the monopolar model. However, these arguments are not supported by the quantum-chemical simulations which predict the asymmetry in the electronic structure of the oxygen vacancy on ZrO_2 with a trapped electron and hole [16].

5. Conclusion

In conclusion, the trap nature in ZrO_2 was studied with EPR spectroscopy and charge transport experiments and simulations. It was established that the oxygen vacancies act as the traps responsible for the charge transport in ZrO_2. Both electrons and holes might be localized on the oxygen vacancies in ZrO_2. The charge transport in ZrO_2 is limited by the phonon-assisted tunneling between traps. The thermal $W_t = 1.25$ eV and optical $W_{opt} = 2.5$ eV trap energies in ZrO_2 were determined. Thus, it can be concluded that the oxygen vacancies in ZrO_2 are responsible for the transport. It was shown that the X-ray irradiation of ZrO_2 films on a silicon substrate transforms interstitial oxygen atoms and oxygen vacancies into a paramagnetic state, and the observed parameters of the EPR spectra correspond to the data for these centres. However, the role of interstitial oxygen atoms in the charge transport and luminescence properties is not clear and is the subject of further studies.

Author information

ORCID
Damir R. Islamov: 0000-0002-5188-7049
Vladimir A. Gritsenko: 0000-0003-1646-0848
Timofey V. Perevalov: 0000-0003-0895-6202
Vladimir Sh. Aliev: 0000-0002-4266-971X

Declaration of Competing Interest

The authors declare no competing interests. The authors declare that they have no known competing financial interests or personal relationships that could have appeared to influence the work reported in this paper.

Acknowledgments

This work was partly supported by the Russian Science Foundation under grant No. 16-19-00002 (quantum chemical simulations, transport measurements and simulations), and partly supported by the ISP

SB RAS state research program, project No. 0306-2019-0005 (EPR spectroscopy). The simulations were performed using computing clusters of the Rzhanov Institute of Semiconductor Physics SB RAS and Novosibirsk State University.

References

[1] T.V. Perevalov, V.A. Gritsenko, Application and electronic structure of high-permittivity dielectrics, Phys.-Usp. 53 (6) (2010) 561–575, doi:10.3367/UFNe.0180.201006b.0587.

[2] J. Robertson, R.M. Wallace, High-K materials and metal gates for CMOS applications, Mater. Sci. Eng. R: Rep. 88 (2015) 1–41, doi:10.1016/j.mser.2014.11.001.

[3] S. Monaghan, K. Cherkaoui, E. O'Connor, V. Djara, P.K. Hurley, L. Oberbeck, E. Tois, L. Wilde, S. Teichert, TiN/ZrO_2/Ti/Al metal–insulator–metal capacitors with sub-nanometer CET using ALD-deposited ZrO_2 for DRAM applications, IEEE Electron Dev. Lett. 30 (3) (2009) 219–221, doi:10.1109/led.2008.2012356.

[4] G. Congedo, A. Lamperti, L. Lamagna, S. Spiga, Stackengineering of TANOS charge-trap flash memory cell using high-$\kappa$$ZrO_2$ grown by ALD as charge trapping layer, Microelectron. Engi. 88 (2011) 1174–1177, doi:10.1016/j.mee.2011.03.066. https://www.sciencedirect.com/science/article/pii/S016793171100325X.

[5] V.A. Gritsenko, Y.N. Novikov, T.V. Perevalov, V.N. Kruchinin, V.S. Aliev, A.K. Gerasimova, S.B. Erenburg, S.V. Trubina, K.O. Kvashnina, I.P. Prosvirin, M. Lanza, Nanoscale potential fluctuations in zirconium oxide and the flash memory based on electron and hole localization, Adv. Electron. Mater. 4 (2018) 1700592, doi:10.1002/aelm.201700592.

[6] J. Lee, E.M. Bourim, W. Lee, J. Park, M. Jo, S. Jung, J. Shin, H. Hwang, Effect of ZrO_x/HfO_x bilayer structure on switching uniformity and reliability in nonvolatile memory applications, Appl. Phys. Lett. 97 (2010) 172105, doi:10.1063/1.3491803.

[7] S.-Y. Wang, D.-Y. Lee, T.-Y. Tseng, C.Y. Lin, Effects of Ti top electrode thickness on the resistive switching behaviors of rf-sputtered ZrO_2 memory films, Appl. Phys. Lett. 95 (2009) 112904, doi:10.1063/1.3231872.

[8] X. Wu, P. Zhou, J. Li, L.Y. Chen, H.B. Lv, Y.Y. Lin, T.A. Tang, Reproducible unipolar resistance switching in stoichiometric ZrO_2 films, Appl. Phys. Lett. 90 (2007) 183507, doi:10.1063/1.2734900.

[9] C.B. Azzoni, A. Paleari, EPR study of electron traps in X-ray-irradiated yttria-stabilized zirconia, Phys. Rev. B 40 (10) (1989) 6518–6522, doi:10.1103/physrevb.40.6518.

[10] J.X. Zheng, G. Ceder, T. Maxisch, W.K. Chim, W.K. Choi, First-principles study of native point defects in hafnia and zirconia, Phys. Rev. B 75 (2007) 104112, doi:10.1103/PhysRevB.75.104112.

[11] J. Aarik, H. Mändar, M. Kirm, Spectroscopic characterization of ZrO_2 thin films grown by atomic layer deposition, Proc. Est. Acad. Sci. Phys. Math. 52 (3) (2003) 289–298.

[12] A.S. Foster, V.B. Sulimov, F. Lopez Gejo, A.L. Shluger, R.M. Nieminen, Structure and electrical levels of point defects in monoclinic zirconia, Phys. Rev. B 64 (2001) 224108, doi:10.1103/PhysRevB.64.224108. https://journals.aps.org/prb/abstract/10.1103/PhysRevB.64.224108.

[13] C. Århammar, C.M. Araújo, R. Ahuja, Energetics of Al doping and intrinsic defects in monoclinic and cubic zirconia: first-principles calculations, Phys. Rev. B 80 (2009) 115208, doi:10.1103/PhysRevB.80.115208. http://link.aps.org/doi/10.1103/PhysRevB.80.115208.

[14] J.-H. Hur, S. Park, U.I. Chung, First principles study of oxygen vacancy states in monoclinic ZrO_2: interpretation of conduction characteristics, J. Appl. Phys. 112 (11) (2012) 113719, doi:10.1063/1.4768894.

[15] T.V. Perevalov, D.R. Islamov, Oxygen polyvacancies as conductive filament in zirconia: first principle simulation, ECS Trans. 80 (2017) 357–362, doi:10.1149/08001.0357ecst. http://ecst.ecsdl.org/content/80/1/357.

[16] D.R. Islamov, V.A. Gritsenko, T.V. Perevalov, A.P. Yelisseyev, V.A. Pustovarov, I.V. Korolkov, E.E. Lomonova, Oxygen vacancies in zirconium oxide as the blue luminescence centres and traps responsible for charge transport: Part I—crystals, Materialia (2021), doi:10.1016/j.mtla.2020.100979. https://www.sciencedirect.com/science/article/abs/pii/S2589152920303951.

[17] Z.A. Weinberg, Tunneling of electrons from Si into thermally grown SiO_2, Solid-State Electron. 20 (1) (1977) 11–18, doi:10.1016/0038-1101(77)90027-2. https://www.sciencedirect.com/science/article/pii/0038110177900272.

[18] N. Novikov, V.A. Gritsenko, K.A. Nasyrov, Charge transport mechanism in amorphous alumina, Appl. Phys. Lett. 94 (2009) 222904, doi:10.1063/1.3151861. http://aip.scitation.org/doi/10.1063/1.3151861.

[19] D.R. Islamov, V.A. Gritsenko, C.H. Cheng, A. Chin, Bipolar conductivity in amorphous HfO_2, Appl. Phys. Lett. 99 (2011) 072109, doi:10.1063/1.3626599.

[20] T. Ando, N.D. Sathaye, K.V.R.M. Murali, E.A. Cartier, On the electron and hole tunneling in a HfO_2 gate stack with extreme interfacial-layer scaling, IEEE Electron Dev. Lett. 32 (7) (2011) 865–867, doi:10.1109/LED.2011.2146751.

[21] V.A. Gritsenko, T.V. Perevalov, D.R. Islamov, Electronic properties of hafnium oxide: a contribution from defects and traps, Phys. Rep. 613 (2016) 1–20, doi:10.1016/j.physrep.2015.11.002.

[22] D.R. Islamov, T.V. Perevalov, V.A. Gritsenko, C.H. Cheng, A. Chin, Charge transport in amorphous $Hf_{0.5}Zr_{0.5}O_2$, Appl. Phys. Lett. 106 (2015) 102906 1501.02370, doi:10.1063/1.4914900.

[23] D.R. Islamov, V.A. Gritsenko, C.H. Cheng, A. Chin, Bipolar conductivity in nanocrystallized TOo_2, Appl. Phys. Lett. 101 (2012) 032101, doi:10.1063/1.4737016.

[24] D.R. Islamov, V.A. Gritsenko, C.H. Cheng, A. Chin, Evolution of the conductivity type in Germania by varying the stoichiometry, Appl. Phys. Lett. 103 (2013) 232904, doi:10.1063/1.4838297.

[25] T.V. Perevalov, D.V. Gulyaev, V.S. Aliev, K.S. Zhuravlev, V.A. Gritsenko, A.P. Yelisseyev, The origin of 2.7 eV blue luminescence band in zirconium oxide, J. Appl. Phys. 116 (2014) 244109, doi:10.1063/1.4905105.

[26] S. Li, W.T. Zheng, Q. Jiang, Size and pressure effects on solid transition temperatures of ZrO_2, Scr. Mater. 54 (2006) 2091–2094, doi:10.1016/j.scriptamat.2006.03.002.

[27] F.H. Hielscher, H.M. Preier, Non-equilibrium C-V and I-V characteristics of metal-insulator-semiconductor capacitors, Solid-State Electron. 12 (1969) 527–538, doi:10.1016/0038-1101(69)90108-7.

[28] V.A. Gritsenko, E.E. Meerson, On silicon nitride conductivity, Phys. Status Solidi A 62 (1980), doi:10.1002/pssa.2210620252. K131–K134

[29] A.S. Ginovker, V.A. Gritsenko, S.P. Sinitsa, Two-band conduction of amorphous silicon nitride, Phys. Status Solidi A 26 (1974) 489–495, doi:10.1002/pssa.2210260211.

[30] Y.N. Novikov, V.A. Gritsenko, Relaxation of the electric current in Si_3N_4: experiment and numerical simulation, Phys. Solid State 59 (2017) 47–52, doi:10.1134/S1063783417010255.

[31] A.A. Pil'nik, A.A. Chernov, D.R. Islamov, Charge transport mechanism in dielectrics: drift and diffusion of trapped charge carriers, Sci. Rep. 10 (2020) 15759, doi:10.1038/s41598-020-72615-1.

[32] K.A. Nasyrov, V.A. Gritsenko, Charge transport in dielectrics via tunneling between traps, J. Appl. Phys. 109 (2011) 093705, doi:10.1063/1.3587452. [cited 2013.06.19]

[33] D.R. Islamov, V.A. Gritsenko, C.H. Cheng, A. Chin, Origin of traps and charge transport mechanism in hafnia, Appl. Phys. Lett. 105 (22) (2014) 222901 1409.6887, doi:10.1063/1.4903169.

[34] D.R. Hamann, Optimized norm-conserving vanderbilt pseudopotentials, Phys. Rev. B 88 (2013) 085117, doi:10.1103/physrevb.88.085117.

[35] D.R. Hamann, Erratum: optimized norm-conserving vanderbilt pseudopotentials [Phys. Rev. B 88, 085117 (2013)], Phys. Rev. B 95 (2017) 239906, doi:10.1103/physrevb.95.239906.

[36] P. Giannozzi, O. Andreussi, T. Brumme, O. Bunau, M.B. Nardelli, M. Calandra, R. Car, C. Cavazzoni, D. Ceresoli, M. Cococcioni, N. Colonna, I. Carnimeo, A.D. Corso, S. de Gironcoli, P. Delugas, R.A. DiStasio, A. Ferretti, A. Floris, G. Fratesi, G. Fugallo, R. Gebauer, U. Gerstmann, F. Giustino, T. Gorni, J. Jia, M. Kawamura, H.-Y. Ko, A. Kokalj, E. Küçükbenli, M. Lazzeri, M. Marsili, N. Marzari, F. Mauri, N.L. Nguyen, H.-V. Nguyen, A.O.-d.l. Roza, L. Paulatto, S. Poncé, D. Rocca, R. Sabatini, B. Santra, M. Schlipf, A.P. Seitsonen, A. Smogunov, I. Timrov, T. Thonhauser, P. Umari, N. Vast, X. Wu, S. Baroni, Advanced capabilities for materials modelling with Quantum ESPRESSO, J. Phys.: Condens. Matter 29 (46) (2017) 465901, doi:10.1088/1361-648x/aa8f79.

[37] S. Kondo, T. Sumi, T. Seki, Drastically enhanced optical absorption in quench-deposited amorphous CuI films, Phys. Status Solidi (B) 184 (2) (1994), doi:10.1002/pssb.2221840236. K57–K61

[38] R. Zallen, The Physics of Amorphous Solids, Wiley, VCH, 1998. https://www.ebook.de/de/product/4252406/richard_zallen_the_physics_of_amorphous_solids.html.

[39] G. Jegert, A. Kersch, W. Weinreich, U. Schröder, P. Lugli, Modeling of leakage currents in high-κ dielectrics: three-dimensional approach via kinetic Monte Carlo, Appl. Phys. Lett. 96 (6) (2010) 062113, doi:10.1063/1.3310065.

[40] D.R. Islamov, V.A. Gritsenko, T.V. Perevalov, O.M. Orlov, G.Y. Krasnikov, The charge transport mechanism and electron trap nature in thermal oxide on silicon, Appl. Phys. Lett. 109 (2016) 052901, doi:10.1063/1.4960156.

[41] V.M. Orera, R.I. Merino, Y. Chen, R. Cases, P.J. Alonso, Intrinsic electron and hole defects in stabilized zirconia single crystals, Phys. Rev. B 42 (16) (1990) 9782–9789, doi:10.1103/physrevb.42.9782.

[42] E.V. Frolova, M.I. Ivanovskaya, The origin of defects formation in nanosized zirconia, Mater. Sci. Eng.: C 26 (2006) 1106–1110, doi:10.1016/j.msec.2005.09.016.

[43] C. Gionco, M.C. Paganini, E. Giamello, R. Burgess, C.D. Valentin, G. Pacchioni, Paramagnetic defects in polycrystalline zirconia: an EPR and DFT study, Chem. Mater. 25 (11) (2013) 2243–2253, doi:10.1021/cm400728j.

[44] V.V. Afanas'ev, A. Stesmans, Internal photoemission at interfaces of high-κ insulators with semiconductors and metals, J. Appl. Phys. 102 (2007) 081301, doi:10.1063/1.2799091.

[45] V.V. Afanas'ev, M. Houssa, A. Stesmans, M.M. Heyns, Band alignments in metal-oxide-silicon structures with atomic-layer deposited Al_2O_3 and ZrO_2, J. Appl. Phys. 91 (2002) 3079–3084, doi:10.1063/1.1436299.

[46] W. Schottky, Über den einfluß von strukturwirkungen, besonders der thomsonschen bildkraft, auf die elektronenemission der metalle, Phys. Z. 15 (1914) 872–878.

[47] D.V. Gritsenko, S.S. Shaĭmeev, M.A. Lamin, O.P. Pcheljakov, V.A. Gritsenko, V.G. Lifshits, Two-band conductivity of ZrO_2 synthesized by molecular beam epitaxy, JETP Lett. 81 (2005) 587–589, doi:10.1134/1.2029950.

[48] J. Frenkel, On the theory of electric breakdown of dielectrics and electronic semiconductors, Tech. Phys. USSR 5 (1938) 685–695.

[49] D.R. Islamov, A.G. Chernikova, M.G. Kozodaev, A.M. Markeev, T.V. Perevalov, V.A. Gritsenko, O.M. Orlov, Charge transport mechanism in thin films of amorphous and ferroelectric $Hf_{0.5}Zr_{0.5}O_2$, JETP Lett. 102 (2015) 544–547, doi:10.1134/S0021364015200047.